Myristylation of FBR v-fos Dictates the Differentiation Pathways in Malignant Osteosarcoma

Robert M. Jotte and Jeffrey T. Holt

Department of Cell Biology, Vanderbilt University Medical Center, Nashville, Tennessee 37232

Abstract. Myristylation of FBR v-fos, a c-fos retroviral homologue that causes osteosarcomas in mice, determines many of its transcriptional properties in vitro. To determine whether myristylation of FBR v-fos contributes to in vivo tumorigenicity, we examined its transforming capability in comparison to a nonmyristylated FBR v-fos (G2A-R). Retroviral infections with FBR v-fos and G2A-R transform BALB/c-3T3 cells. The number, size, and cellular morphology of foci generated by both FBR and G2A-R are indistinguishable. However, marked biological differences were found in transgenic mice expressing either the myristylated FBR v-fos or the nonmyristylated G2A-R. 11 of 26 FBR v-fos transgenic mice died as a result of gross tumor burden. None of the 28 G2A-R transgenic mice died from tumor burden, and only two of the G2A-R mice developed bone tumors. Histologic examination of the tumors reveals that the FBR v-fos bone tumors contain malignant cells with features of four cell lineages (osteocytes, chondrocytes, myocytes, and adipocytes) in an environment rich in extracellular matrix (ECM). However, the G2A-R tumors exist in an environment devoid of ECM and display malignant cells with features of adipocytes. Masson staining reveals that the ECM of the FBR tumors stains strongly for collagen. Immunohistochemical staining with collagen III antibody demonstrates an abundance of collagen III expression in this ECM. While NH_2-terminal myristylation is not required for FBR immortalization and transformation, it is essential in determining the degree of differentiation and tumorigenicity of malignant cells.

THE Finkel-Biskis-Reilly mouse osteosarcoma virus (FBR-MuSV)[1] was originally isolated from a radiation induced bone tumor in an XG/f mouse (Finkel et al., 1975). FBR v-fos causes chondro-osseous sarcomas when injected into newborn mice (Ward and Young, 1976; Lee et al., 1979; Michiels et al., 1984; Silbermann et al., 1987). FBR v-fos integration into the host chromosome and constitutive expression following infection (Van Beveren et al., 1984; Meijlink et al., 1985) leads to the transformed phenotype observed in established murine fibroblasts as well as in nonestablished mouse connective tissue cells (Jenuwein et al., 1985; Jenuwein and Müller, 1987).

FBR v-fos is expressed as a 75-kD nuclear protein that differs from c-Fos by deletion and replacement of both NH_2- and COOH-terminal regions with retroviral gag and mouse fox sequences, respectively (Curran and Verma, 1984; Van Beveren et al., 1984; Wilson and Treisman,

1988). FBR v-fos represents an important model in the study of carcinogenesis, since its cellular analogue (c-Fos) is a transcriptional regulator whose early expression is implicated in cellular growth and differentiation. Previously we have shown that FBR v-fos demonstrates both losses of function (inability to transactivate from AP-1 sites and inability to repress from the serum response element in the c-fos promoter) and gains of function (transcriptional activation of the collagen III promoter) when compared to c-Fos (Kamata et. al., 1991; Kamata and Holt, 1992; Jotte et al., 1994). The expression of collagen III, which is normally tightly controlled during the differentiation of 3T3-L1 adipocytes, is markedly disrupted by the presence of FBR v-fos (Jotte et al., 1994). These altered transcriptional properties of FBR v-fos are dependent upon its myristylated NH_2-terminal glycine. A nonmyristylated point mutant FBR protein, G2A-R (for glycine to alanine at the second amino acid site), not only regains its ability to transactivate from AP-1 sites and repress at the serum response element, but it also loses its ability to disrupt the differentiation-dependent expression of collagen III. Absence of myristylation therefore restores FBR's molecular mechanisms to that of its normal cellular homologue, c-Fos.

While myristylation is essential for the differentiation-dependent transcriptional properties of FBR in vitro, its

Address all correspondence to Jeffrey T. Holt, Department of Cell Biology, Vanderbilt University Medical Center, Nashville, TN 37232. Tel.: (615) 343-4730. Fax: (615) 343-5791. E-mail: jeff.holt@mcmail.vanderbilt.edu

R.M. Jotte's current address is Colorado University Health Center, Denver, Colorado.

1. *Abbreviations used in this paper:* ECM, extracellular matrix; FBR-MuSV, Finkel-Biskis-Reilly mouse osteosarcoma virus.

functions through the process of immortalization and tumorigenesis remain undefined. To address the biological relevance of FBR v-fos myristylation, we examined FBR and G2A-R's ability to transform mouse fibroblasts in tissue culture. Myristylation's contribution to tumorigenicity was further characterized in vivo in transgenic mice expressing either the myristylated or nonmyristylated FBR proteins.

Materials and Methods

Cell Cultures and Transfections

FBR v-fos 3T3-L1 stable cell lines and BALB/c-3T3 cells were grown in DME supplemented with 10% FCS (Sigma Chemical Co., St. Louis, MO), 2 mM L-glutamine (Sigma Chemical Co.), and 1× antibiotic/antimycotic (Sigma Chemical Co.). Bosc 23 cells were maintained in DME containing 10% dialyzed FCS, 0.25 mg/ml xanthine (Sigma Chemical Co.), 2 μg/ml aminopterin (Sigma Chemical Co.), 6 μg/ml thymidine (Sigma Chemical Co.), 25 μg/ml mycophenolic acid (GIBCO BRL, Gaithersburg, MD), 2 mM L-glutamine, and 1× antibiotic/antimycotic. 3T3-L1 cells were transfected as proliferating fibroblasts at 30% confluency. Cells were transfected with 10 μg of MuSV-FBR expression vector and 1 μg of RSV-neomycin resistance gene by the calcium phosphate–DNA coprecipitation with glycerol shock (Graham and van der Eb, 1973). After glycerol shock, cells were refed in DME with 10% FCS. 24 h later, transfected cells were split 1:10 and replenished in DME with 10% FCS and 100 μg/ml G418. Cells were maintained in tissue culture in the presence of G418 for 3 wk at which time colonies were isolated and screened for FBR v-fos expression by Western blot.

Generation of FBR and G2A-R Transient Supernatants

G2A-R viral vector was generated by inserting the NcoI fragment of MuSV LTR-driven G2A-R (Kamata and Holt, 1992) into FBR v-fos. 20 μg of FBR or G2A-R was transiently transfected into Bosc 23 cells (plated at a density of 5 × 10⁵ cells the day before) by the calcium phosphate coprecipitation method. 12 h after transfection, media (DME with 10% FCS) was replaced. 48 h after transfection, viral supernatant was harvested and spun at 3,000 rpm to remove cellular debris. Viral supernatants were stored at −70°C.

Titering of FBR and G2A-R Viral Supernatants

For titering by viral RNA hybridization, 20 ml of media in which the viral-producing Bosc 23 cells were growing was centrifuged at 4°C at 10,000 rpm to pellet any producer cells. Supernatants were transferred to a SW27 polyallomer tube and spun for 2 h at 27,000 rpm at 4°C. Viral particles were resuspended in 0.5 ml of 10 mM Tris-HCl, pH 7.5. Viral suspensions were layered onto a 4-ml step gradient in SW50.1 tubes consisting of 2 ml 25% sucrose in 100 mM Tris-HCl, pH 7.5, 1 ml 40% sucrose in 100 mM Tris-HCl, pH 7.5, and 1 ml 50% sucrose in 100 mM Tris-HCl, pH 7.5. Viral suspensions were centrifuged 3 h at 35,000 rpm at 4°C. Viruses resting at the 40% sucrose cushion were phenol–chloroform extracted twice and once with chloroform. RNA was precipitated with an equal volume of isopropanol. Precipitated RNA was resuspended in 250 μl of 15% formaldehyde and 250 μl of 20× SSC. Suspended RNA was heated at 50°C for 15 min and transferred to an ice bath. Serial dilutions in 10× SSC of each sample were made and adsorbed onto a Gene Screen Plus membrane (Dupont/NEN, Wilmington, DE) through a dot blot minifold apparatus. Blots were rinsed in 2× SSC and allowed to air dry. Blots were then baked at 80°C for 2 h to reverse the formaldehyde reaction. RNA transcripts were hybridized with T7 RNA polymerase generated antisense FBR v-fos coding sequence at 60°C and washed according to the protocol provided by the Gene Screen Plus manufacturers.

FBR and G2A-R Transformation Assays in BALB/c-3T3 Cells

2 × 10⁵ BALB/c-3T3 cells were plated per 10-cm dish the day before infection. Serially diluted viral supernatants (10⁻¹, 10⁻², 10⁻³, 10⁻⁴, and 10⁻⁵) were added to BALB/c-3T3 cells in the presence of 6 μg/ml polybrene. The following day, plates were split 1 to 10 and allowed to grow in DME, 10% FCS with a media change every 3 d. At 3 wk, cells were stained with Giemsa stain and scored for foci formation. Foci >5 mm in diameter were scored as positive.

Establishment of Transgenic Mouse Lines

The DNAs injected were the BamHI-XhoI fragment of either the FBR or G2A-R expression vectors that encompassed the Moloney Leukemia virus LTR and the oncogenic region extending through the polyadenylation site (Van Beveren, 1984). Transgenic mice were established through the Vanderbilt University Cancer Center Transgenic Mouse Core. C57BL6 × DBA F1 fertilized eggs were injected with either MuSV-LTR driven FBR or G2A-R encoding DNA (Hogan et al., 1986). At 2 wk of age, mice had 0.5 in of their tails resected and placed into 300 μl of buffer containing 50 mM Tris, pH 8.0, 100 mM EDTA, 100 mM NaCl, 1% SDS, and 175 g proteinase K (Boehringer Mannheim Corp., Indianapolis, IN). Tails were incubated for 12 h at 55°C and then extracted with an equal volume of phenol and chloroform. Precipitated DNA was spooled and resuspended into sterile distilled H₂0. Transmission of the FBR and G2A-R genes in founder and progeny mice was confirmed by PCR analysis of mouse tail DNA using 5'-CAGAGCGGGAATGGTGAAGA-3' and 5'-TGATGC-CGGAAACAAGAAGT-3' oligonucleotides as PCR primers. Founder mice were crossed with C57BL6 nontransgenic mice to determine germline transmission, and progeny mice were screened by PCR as described above.

Tumor Detection, Histology, and Immunohistochemistry

Tumors were initially detected roentgenographically on a General Electric MSI.1250 IV Radiographic Imager (Milwaukee, WI) at settings of 1.5 kV and 1.5 mA. Tumors were resected from the transgenic mice and immersed in 3.7% formaldehyde. Tumors were then embedded in low melting point Ameraffin (Baxter, Marietta, GA) and sectioned at 4–5 μm on a Reichert-Jung microtome. Processing was conducted according to standard procedure by the Vanderbilt University Medical Center Research Management Service. Standard Mayers hematoxylin (Fisher Scientific, Pittsburgh, PA) and pholxine B/eosin y (Fisher Scientific), Masson trichrome (Fisher Scientific), and Sudan black B (Chroma-Gesellschaft, Germany) stains were conducted on paraffin-embedded sections. Immunohistochemistry was conducted on an automated stainer (model Techmate; Biotech Res. Labs, Inc., Rockville, MD) using a universal ABC detection kit with DAB chromagen using the following antibodies: actin prediluted monoclonal antibody (Enzo Biochem Inc., New York), cytokeratin cam 5.2 monoclonal antibody (Becton-Dickinson Immunocytometry Sys., Mountain View, CA) diluted 1:20, desmin monoclonal antibody (Dako Corp., Corpinteria, CA) diluted 1:500, and a rabbit anti–rat collagen type III antibody (Pasteur Institute, Lyon, France) diluted 1:20.

Tumor RNA Isolation and Reverse Transcriptase PCR

RNA was purified from resected tumor tissue as previously described (Chirgwin et al., 1979). Tumors were resected and quick-frozen in liquid N₂. 10 ml of 4 M guanidinium isothiocyanate, 50 mM Tris, 10 mM EDTA solution was added per gram of tissue, and tissue was ground with a tissuemizer. Suspensions were centrifuged 10 min at 10,000 rpm at 12°C, and supernatants were heated to 65°C for 2 min in the presence of 2% Sarkosyl. CsCl was then added at a concentration of 0.1 g/ml solution and layered over 5 ml of 5.7 M CsCl in a SW-28 polyallomer tube. Samples were spun overnight at 25,000 rpm at 22°C. RNA pellets were resuspended in 5 mM EDTA, 0.5% Sarkosyl, and 5% 2-mercaptoethanol. Samples were extracted with equal volumes of phenol/chloroform/isoamyl alcohol and precipitated. Quantity and quality of RNA was determined by spectrophotometric ultraviolet light absorbance at 260 nm and by ethidium bromide staining for ribosomal RNA within the total RNA samples. 5 μg total RNA from each sample was treated with 5 U RNAse-free DNAse I (Promega Corp., Madison, WI) at 37°C for 30 min. Samples were extracted with an equal volume of phenol and chloroform and ethanol precipitated. RT-PCR was performed by our published methods (Thompson et al., 1995) using the following basic method: RNA samples were reverse transcribed for 1 h at 37°C using 2 μg of total RNA, 1 μg random hexamers (Boehringer Mannheim Corp.), 1× first strand buffer (GIBCO BRL), 0.01 M DTT, 0.5 mM each dATP, dCTP, dGTP, and dTTP and 200 U Superscript II RNaseH-reverse transcriptase (GIBCO BRL). The RNA/DNA duplexes were used as templates for 20-cycle PCR reactions using
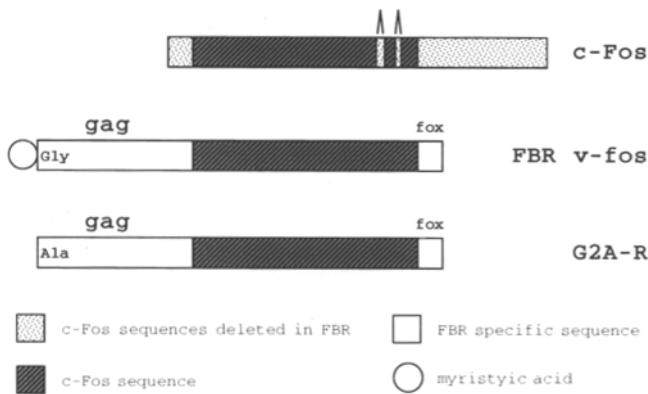
Figure 1. Schematic diagram comparing c-Fos, FBR v-fos, and G2A-R proteins. FBR v-fos differs from c-Fos by both NH_2- and COOH-terminal deletions. These deleted regions are replaced by in-frame Moloney murine sarcoma virus *gag* and mouse *fox* sequences, respectively. FBR v-fos also contains two in-frame deletions of 39 and 27 base pairs, which results in two deletions of 13 and 9 amino acids, respectively, at the COOH terminus. G2A-R differs from FBR in that a single base pair change (G to C) converts the NH_2-terminal glycine (essential for myristylation) to an alanine.

the following conditions: denaturation 94°C, 20 s; annealing 52°C, 45 s; elongation 75°C, 90 s. FBR and G2A-R specific sequences were amplified by PCR with 5'-TTGCCACCCTGCCATGCTAATAA-3' and 5'-CCAC-CGACCTGCCTGCAAGAT-3' primers. These PCR primers detect RNA transcripts spanning the fos and fox regions of the gene that are specific

Table 1. FBR and G2A-R Retroviral Titers by Foci Assay Formation in BALB/c-3T3 Cells

	10^{-4} Dilution	10^{-3} Dilution	10^{-2} Dilution
FBR	43	420	4134
G2A-R	46	445	4578

FBR and G2A-R retroviruses were generated as described in Materials and Methods. Dilutions were made from the retroviral stocks. 10^6 logarithmically growing BALB/c-3T3 cells were infected with 1 ml of the respective dilutions in the presence of polybrene. 12 h after infection, plates were passaged 1:10 and allowed to grow for 3 wk. Colony foci were scored as positive if colony diameter was ≥2 mm. Numbers indicate the number of viral particles per ml of initial infecting dilution and represent the average of three separate infections.

for the viral oncogene, 2534 to 2719 from the published sequence (Van Beveren et al., 1984). 20% of PCR products were run on a 2% agarose gel and visualized with ethidium bromide intercalation and UV lighting.

Results

Transformation by FBR is Myristylation Independent

To address the biological relevance of FBR v-fos myristylation, retroviral vectors encoding myristylated FBR v-fos and non-myristylated G2A-R (Fig. 1) were generated as described in Materials and Methods. The FBR v-*fos* and G2A-R retroviral vectors were transiently transfected into Bosc 23 cells (which harbor the Moloney-murine leukemia helper virus) by the calcium phosphate coprecipitation method (Graham and van der Eb, 1973). Viral supernatants were harvested and stored at −70°C. Viral RNA was
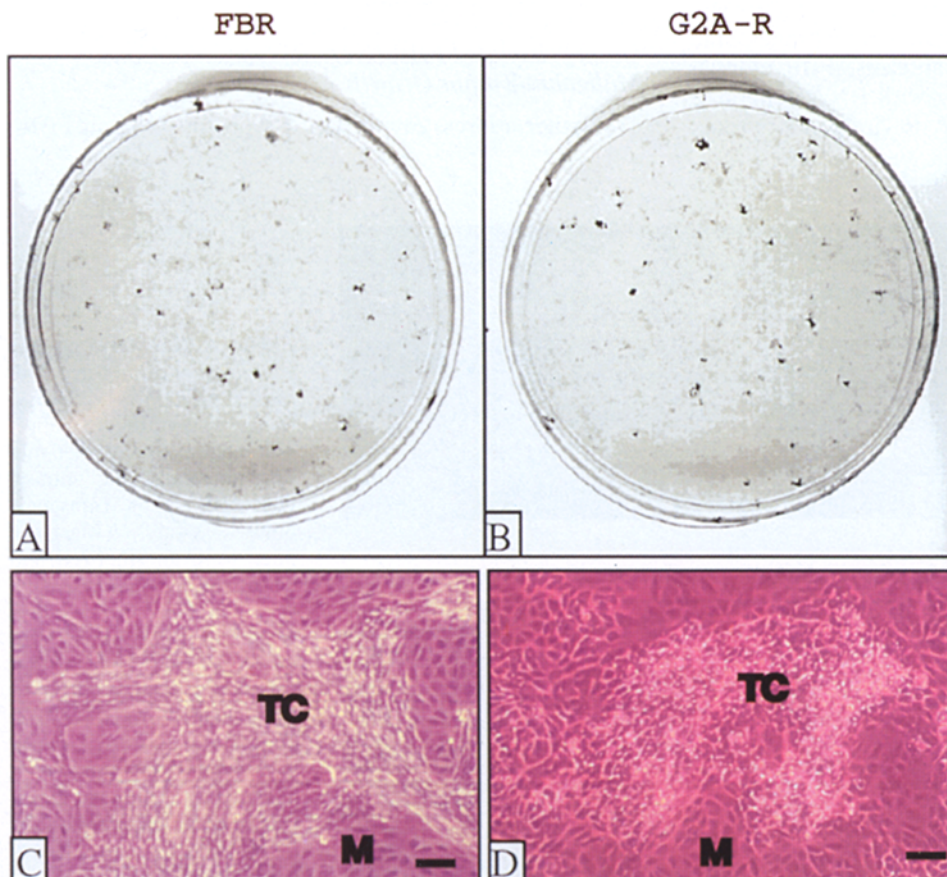

Figure 2. Transformation assay by FBR and G2A-R retroviruses in BALB/c-3T3 fibroblasts. 10^6 logarithmically growing BALB/c-3T3 cells were infected with 10^3 retrovirus particles. 12 h after infection, plates were passaged 1 to 10 and maintained in tissue culture for 3 wk. (*A* and *B*) Giemsa stain of gross FBR and G2A-R transformed colonies, respectively. (*C* and *D*) Cellular morphology of FBR and G2A-R transformed colonies, respectively. *TC*, transformed colony. *M*, BALB/c-3T3 monolayer. 200 magnification. Bar, 20 μm.
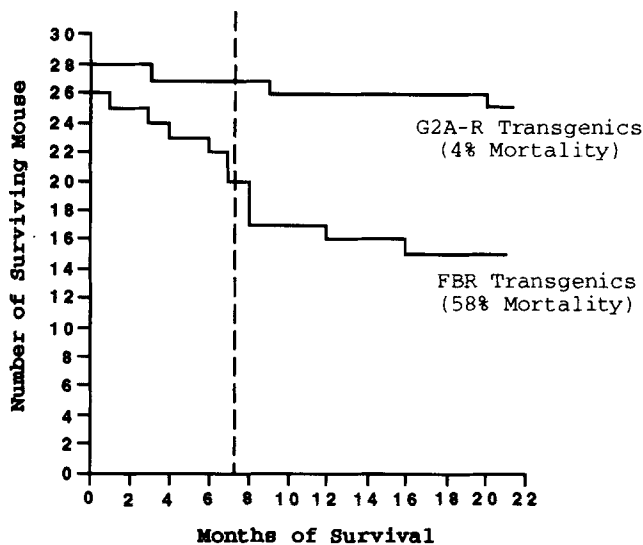
Figure 3. FBR and G2A-R transgenic mouse survival. 26 FBR v-fos and 28 G2A-R transgenic mice were generated as described in Materials and Methods. Over the course of 20 mo, 11 of the 26 FBR transgenic mice succumbed to tumor burden and died (a 58% tumor-dependent mortality). Of the 28 G2A-R transgenic mice, only two developed tumors. These mice were sacrificed at 9 and 20 mo for tumor histology studies. The first G2A-R mouse death was secondary to pneumonia at 4 mo of age. This death and the two mice sacrificed for tissue examination were the only G2A-R transgenic deaths (a 4% study mortality). Dotted line, the average age and standard error of 7.3 ± 1.2 mo at which FBR transgenic mice succumbed to tumor burden.

purified from these viral supernatants as described in Materials and Methods, applied to nylon membranes, and subjected to hybridization with an antisense FBR radiolabeled probe capable of hybridizing with RNA generated from both the FBR v-fos and G2A-R viral vectors (data

not shown). An equal number of either FBR v-fos or G2A-R serially diluted virus particles (as determined by the viral RNA assay) were used to infect 5×10^5 BALB/c-3T3 cells. Cells were infected with 10^4, 10^3, or 10^2 virus particles of either FBR v-fos or G2A-R in the presence of polybrene to enhance viral adherence to the plasma membrane. 12 h after infection, BALB/c-3T3 cells were passaged at a 1:10 dilution and maintained in tissue culture for up to 3 wk. At 3 wk, media was aspirated and the plates were stained with Giemsa. Infection with myristylated FBR v-fos as well as nonmyristylated G2A-R retrovirus causes transformation of BALB/c-3T3 cells as determined by foci formation (Fig. 2, A and B). The growth and size of transformed colonies between the two retroviruses are indistinct, and the cellular morphology of the transformed BALB/c-3T3 cells generated by both retroviruses are also very similar (Fig. 2, C and D). An average of three separate foci transformation assays reveals that the number and size of BALB/c-3T3 foci generated by both FBR and G2A-R are indistinguishable (Table I). These experiments demonstrate that FBR and G2A-R retroviruses have functionally indistinct qualitative and quantitative transforming characteristics, indicating that myristylation of FBR v-fos does not affect either its ability or efficiency to cause transformation of fibroblasts. Although the gross morphology of the cells transformed by either the myristylated or nonmyristylated forms appears similar, it is conceivable that a more detailed structural analysis might reveal differences which would correlate with the observed in vivo effects. Prior studies have shown no differences in the actin cytoskeleton of these cells using immunohistochemistry, but more subtle structural effects may be present.

Nonmyristylated FBR (G2A-R) Does Not Cause Malignant Tumor Growth

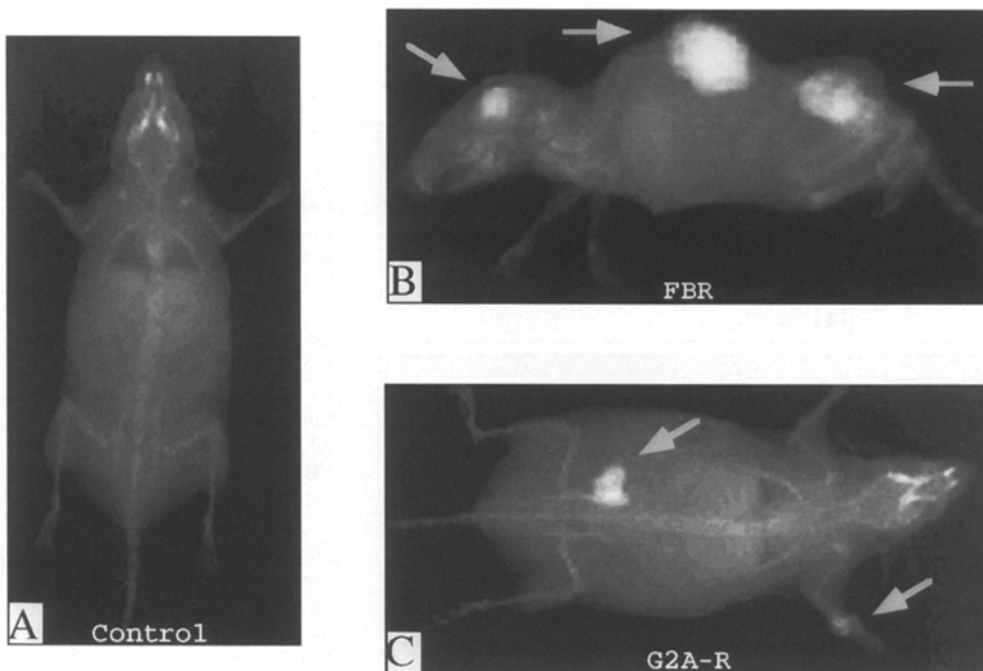To further address myristylation's possible role in FBR's

Figure 4. Roentgenographic examination of transgenic tumors. (A) Control C57/BL6 mouse x-ray. Figure represents a normal x-ray of a 6-mo-old non-transgenic mouse. (B) FBR v-fos transgenic mouse x-ray. Transgenic mice were anesthetized and visualized on a General Electric MSI.1250 IV Radiographic Imager on settings of 1.5 kV and 1.5 mA. Arrows indicate three sites of FBR tumor formation. (C) G2A-R transgenic mouse x-ray. Transgenic mice were anesthetized and visualized as described in B. Arrows indicate two sites of G2A-R tumor formation.

tumorigenic properties, transgenic mice carrying either the myristylated FBR or the non-myristylated G2A-R genes were generated as described in Material and Methods. Carriers of the transgene were confirmed by PCR analysis of DNA isolated from a resected portion of each mouse's tail. PCR analysis was designed to detect both the endogenous c-*fos* gene as well as the exogenous transgene (data not shown). Two FBR and three G2A-R founders were generated from the initial transgenic injections. However, only one FBR and two G2A-R mice from these founders displayed germ-line transmission of the respective transgenes. These founders were mated with nontransgenic B6D2 mice, and F2 progeny were screened for the presence of the transgene by PCR analysis (data not shown). 26 mice harboring the myristylated FBR gene and 28 mice carrying the nonmyristylated G2A-R gene were sired from the corresponding founders and compared for tumor growth and mouse survival.

Marked differences were observed between the FBR and G2A-R transgenics. Of 26 FBR transgenic mice, 11 developed tumors and died over the course of 20 mo. Each of these deaths were secondary to tumor burden. However, of 28 G2A-R transgenic mice, only three died over the same time period. The first G2A-R transgenic mouse death occurred at 3 mo of age and was due to pneumonia; no tumors were detected at autopsy. The two remaining deaths were sacrifices at 9 and 20 mo to examine tumor histology. More importantly, the two G2A-R mice sacrificed for tumor histology were the only two G2A-R transgenic mice that developed tumors. While 11% of the G2A-R mice died during this study, there was only a 4% mortality rate which is attributed to a pneumonia. 0% of the G2A-R transgenic mouse deaths were due to tumor burden. However, 58% of the FBR transgenics died, all of which were deaths caused by tumor burden (Fig. 3). Although the data presented was obtained with a single line of FBR transgenic mice, a second founder (female) developed a large pelvic osteosarcoma which may have contributed to her lack of offspring and proved ultimately fatal. This second founder confirms that FBR v-fos transgenics develop lethal osteosarcomas.

FBR- and G2A-R–induced tumors were initially detected roentgenographically as early as 2 mo of age. Fig. 4 *A* demonstrates a normal roentgenogram from a control nontransgenic mouse. In comparing the FBR and G2A-R tumors, the malignant nature of the FBR tumors compared to that of the G2A-R tumors is readily visible (compare Fig. 4, *B* and *C*). Tumors became grossly detectable as early as 3 mo of age with an average survival of 7.3 ± 1.2 mo in the FBR transgenic mouse group.

To ensure that the tumors isolated from the FBR and G2A-R transgenics did express the respective transgenes, reverse transcriptase polymerase chain reactions specific for FBR and G2A-R sequences were conducted. Total RNA was isolated from the different tumors by cesium chloride purification as described in Materials and Methods and digested with RNAse-free DNAse to ensure samples were not contaminated with DNA. Primers were designed to encompass FBR and G2A-R specific sequences which flank the *fos*/*fox* junction in FBR and G2A-R. Because the amplified region lies near the 3' end of FBR, only completely transcribed message is detected. Fig. 5
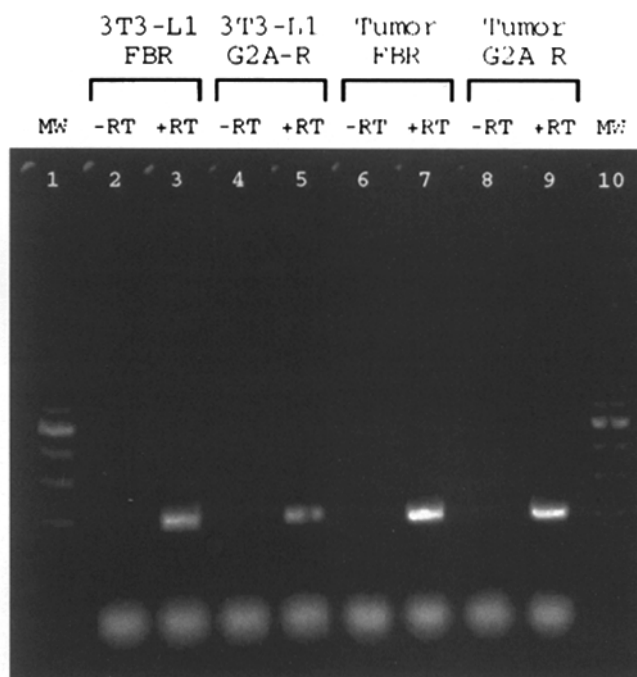

Figure 5. Reverse transcriptase PCR of FBR and G2A-R transcripts isolated from tumors. Reverse transcriptase PCR was performed on total RNA isolated from FBR and G2A-R resected tumors. Equal levels of RNAs were confirmed by spectrophotometric ultraviolet light absorption at 260 nm and by ribosomal staining with ethidium bromide. Samples without reverse transcriptase served as a negative control to ensure that amplified sequences were driven from an RNA template and not DNA. Total RNA isolated from FBR and G2A-R stably transfected 3T3-L1 cell lines served as positive controls. Amplified PCR products were resolved on a 2% agarose gel and visualized by ethidium bromide staining. (Lane *1*) 100-bp molecular weight standards (Promega). (Lane *2*) FBR stably transfected 3T3-L1 cell line negative control, no reverse transcriptase. (Lane *3*) FBR stably transfected 3T3-L1 cell line positive control. (Lane *4*) G2A-R stably transfected 3T3-L1 cell line negative control, no reverse transcriptase. (Lane *5*) G2A-R stably transfected 3T3-L1 cell line positive control. (Lane *6*) FBR tumor RNA negative control, no reverse transcriptase. (Lane *7*) FBR tumor RNA generated PCR product. (Lane *8*) G2A-R tumor RNA negative control, no reverse transcriptase. (Lane *9*) G2A-R tumor RNA generated PCR product. (Lane *10*) Same as Lane *1*.

demonstrates that both the FBR-induced tumors and the G2A-R induced tumors express message for their respective genes (Fig. 5, lanes 7 and 9). Total RNA isolated from 3T3-L1 cell lines stably transfected with the FBR or G2A-R genes served as positive controls (Fig. 5, lanes 3 and 5). Omission of the reverse transcriptase cDNA step served as a negative control to ensure that amplified fragments were not generated from contaminating DNA (Fig. 5, lanes 2, 4, 6, and 8). This study confirms that the FBR and G2A-R tumors express messages encoded by the respective transgenes.

Myristylation of FBR Defines Tumor Histology

Subsequent to the deaths of the FBR transgenic mice, tu-
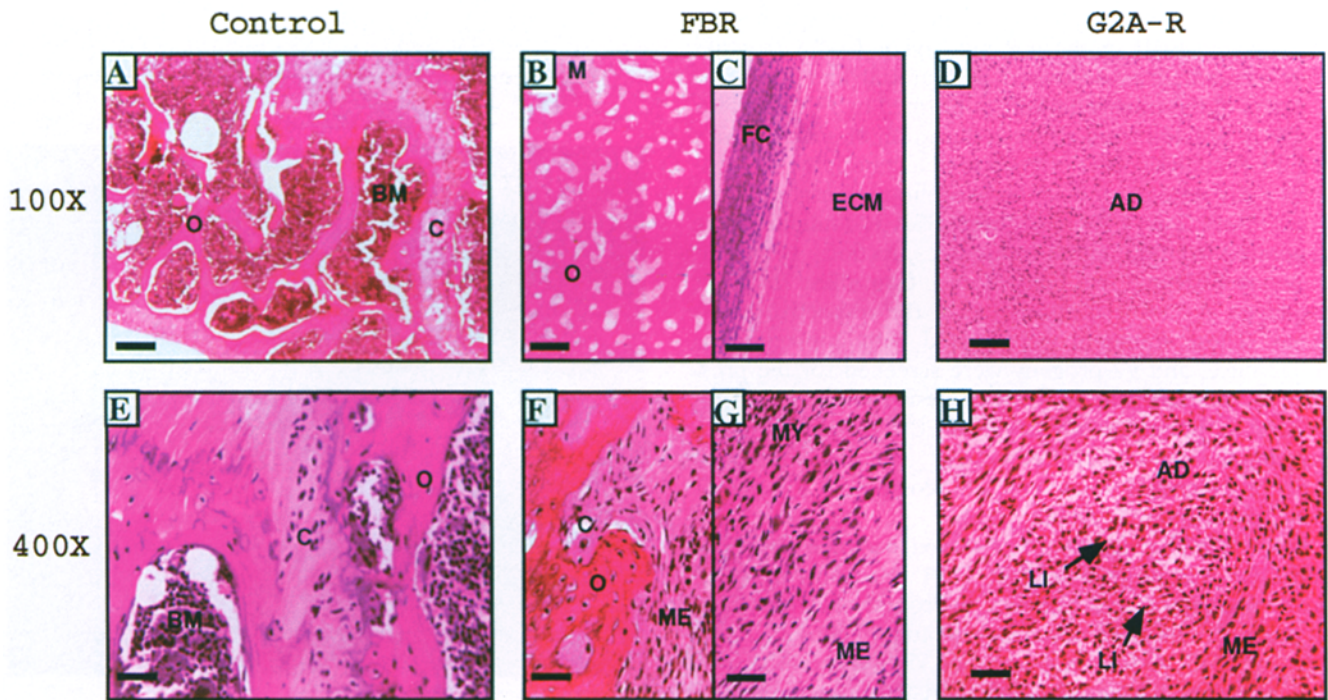
Figure 6. Haematoxylin and eosin stains of FBR and G2A-R tumor sections. (*A*) Control mouse long bone. Femur was isolated from a nontransgenic C57BL6 mouse, fixed, and stained as described in Materials and Methods. *O*, osteocytes within calcified bone; *C*, chondrocytes within cartilage; *BM*, bone marrow. (*B*) Central FBR tumor section. FBR tumors were resected, fixed, and stained as described in Materials and Methods. This section represents a central portion typical of the FBR tumors with osteosarcomatous features (*O*) within calcified bone and discrete regions of soft tissue consisting of poorly differentiated mesenchymal cells (*M*). (*C*) Peripheral FBR tumor section. This is a peripheral section demonstrating the fibrous capsule (*FC*) which surrounds FBR tumors. A soft tissue component is seen just inside the fibrous capsule and is rich in extracellular matrix (*ECM*). (*D*) G2A-R tumor section. This figure is representative of the cellular histology seen throughout the majority of the G2A-R tumors. The tumors are very cellular, representing transformed cells of the adipocyte lineage (*AD*), and devoid of the extracellular matrix seen in FBR tumors. *A–D* 100 magnification. (*E*) Control mouse long bone at high power. Higher magnification of control long bone seen in *A* demonstrates the normal cellular histology consisting of chondrocytes (*C*), osteocytes (*O*), and bone marrow (*BM*). (*F*) Central portion of FBR tumor at high power. This section demonstrates the cellular pattern typical of osteosarcoma (*O*), chondrosarcoma (*C*), and poorly differentiated mesenchymal cells (*ME*) seen in FBR tumors. (*G*) Peripheral section of FBR tumor at high power. This figure reveals the histologic pattern of cells typically seen at the periphery and within the extracellular matrix of FBR tumors. *MY*, myosarcomatous cells; *ME*, poorly differentiated mesenchymal cells. (*H*) G2A-R tumor at high power magnification. This section reveals the poorly differentiated mesenchymal cells (*ME*) and cells representative of the adipocyte-like liposarcomas (*AD*). Arrows point to areas of lipid-laden cells (*LI*). *E–H* 400 magnification. Bars: (*A–D*) 40 μm; (*E–H*) 10 μm.

mors were excised and compared with tumors isolated from the sacrificed G2A-R transgenics. Tumors and normal long bone were fixed in 3.7% formaldehyde, paraffin embedded, and sectioned for histologic examination. Fig. 6, *A* and *E,* is haematoxylin and eosin stains of normal long bone for comparison. H&E staining of FBR tumor sections reveals that these tumors are osteosarcomas (Fig. 6 *B*) with additional features of chondrosarcoma, rhabdomyosarcoma, and liposarcoma. FBR tumors also possess a peripheral band of fibrous tissue which encapsulates the tumor (Fig. 6 *C*). High power views reveal the multiple differentiated features of the FBR osteosarcomas throughout the tumor (Fig. 6, *F* and *G*). G2A-R tumors, however, are liposarcomas and lack features of multiple differentiated cell lineages other than the adipocyte (Fig. 6 *D*). Although the G2A-R liposarcomas possess a large proportion of poorly differentiated mesenchymal cells, there are adipocyte-like cells with lipid-laden vesicles (Fig. 6 *H*). Sudan black staining for lipid and phospholipid reveals that FBR tumors express low levels of lipid, and

G2A-R tumors express significant levels (Fig. 7, *A* and *D*). Immunohistologic stains for actin reveals that FBR tumors stain positive in regions consistent with rhabdomyosarcomatous features (compare Fig. 7, *B* and *C*). However, G2A-R tumors do not stain for actin, confirming that G2A-R tumors lack cells with myocyte-type features (compare Fig. 7, *E* and *F*). Additional stains for cytokeratin were conducted to determine if either the FBR or G2A-R tumors contain cells of epithelial origin. Neither FBR or G2A-R tumors stain positively for cytokeratin (data not shown). Thus, FBR tumors display characteristics with four differentiating features (osteosarcoma, chondrosarcoma, rhabdomyosarcoma, and liposarcoma). However, G2A-R tumors only display features of the differentiating liposarcoma.

Closer examination of the FBR osteosarcomas reveals an abundance of extracellular matrix (ECM) throughout the tumor (Fig. 8 *A*). G2A-R liposarcomas display a largely cellular component that is devoid of the ECM seen in FBR tumors (Fig. 8 *D*). Masson staining of the tumor
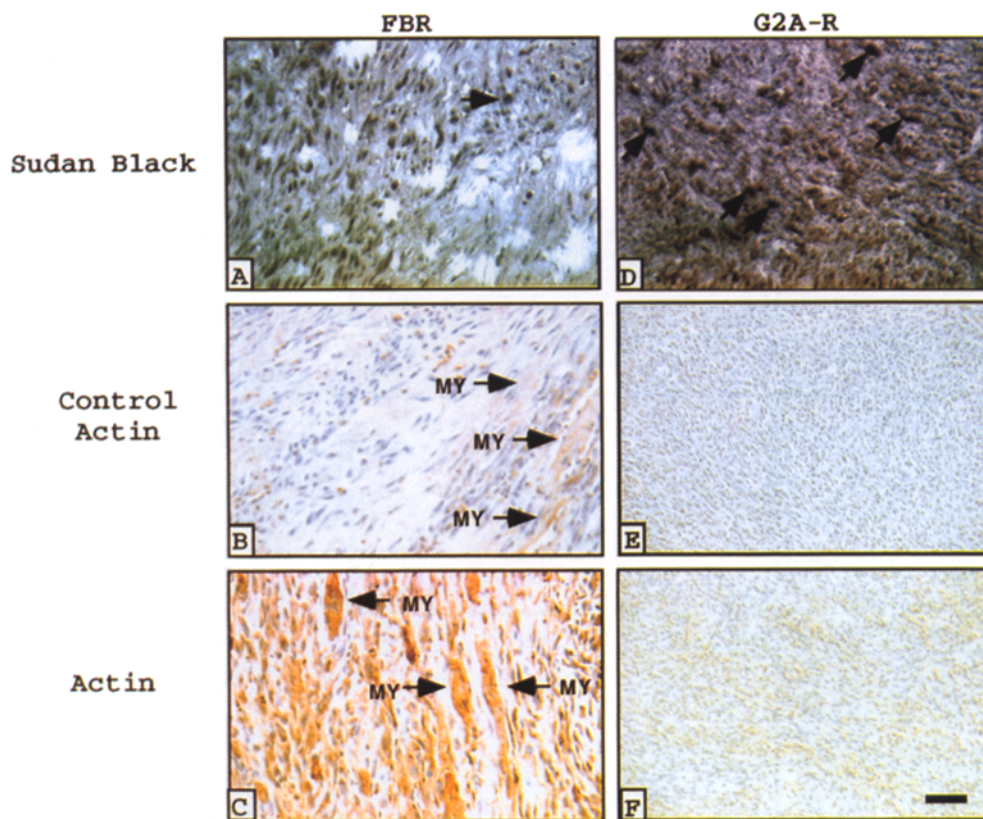
Figure 7. Tissue-specific staining in FBR and G2A-R tumors. (*A*) Sudan black B stain of FBR tumor. FBR tumors were fixed, sectioned, and stained as described in Materials and Methods. Sudan black B detects cells of the adipocyte lineage, as it stains lipids and phospholipids black. The arrow indicates a poorly differentiated mesenchymal cell that stains positively for Sudan black B. (*B*) FBR control actin stain. Section represents the background immunoperoxidase staining pattern observed in FBR tumor sections. This field represents the periphery of the FBR tumor within the extracellular matrix. Arrows indicate myocytes (*MY*) visible in this portion of the FBR tumor. (*C*) Actin staining seen in FBR tumors. Arrows point to actin positive staining, which is seen within cells noted to be myocytes (*MY*). (*D*) Sudan black B stain of G2A-R tumor. G2A-R tumors were fixed, sectioned, and stained as described in Materials and Methods. Note the overall increased staining for Sudan black B throughout the tumor, confirming the adipocyte-like features of the G2A-R liposarcomas. Arrows indicate lipid-laden liposarcoma cells. (*E*) G2A-R control actin stain. Section represents the background immunoperoxidase staining pattern observed in G2A-R tumor sections. (*F*) Actin staining seen in G2A-R tumors. Note the lack of positive staining throughout the G2A-R tumor section, confirming the absence of cells from the myocyte lineage in G2A-R tumors. 400 magnification. Bar, 10 μm.

sections reveals that the high levels of ECM seen in FBR tumors stain strongly for collagen (Fig. 8 *B*). FBR osteosarcomas also contain a fibrous capsule that encompasses the tumor and is rich in collagen (Fig. 8 *C, arrows*). G2A-R tumors not only lack this fibrous capsule, but they also fail to stain for collagen throughout the tumor (Fig. 8 *E*). These studies demonstrate that the FBR tumors that are rich in ECM express high levels of collagen protein, whereas the G2A-R tumors lack ECM and therefore fail to stain for collagen.

Because FBR is known to transcriptionally activate the collagen III promoter (Setoyama et al., 1986a; Jotte et al., 1994), specific immunoperoxidase staining for collagen III was performed on the FBR and G2A-R tumors as described in Materials and Methods. Immunoperoxidase positive staining was greatest at the periphery of the FBR tumors within the fibrous capsule (compare Fig. 9, *A* and *B*). This suggests that the fibrous capsule surrounding the FBR osteosarcomas consists largely of collagen III protein. Higher magnification reveals the extent of ECM-rich FBR osteosarcoma which stains for collagen III protein (compare Fig. 9, *C* and *D*). G2A-R liposarcomas demonstrate a markedly lower level of collagen III protein expression throughout the tumor (compare Fig. 9, *G* and *H*). There is also a lack of enhanced collagen III expression at

the tumor periphery, as the G2A-R liposarcomas lack a fibrous capsule (compare Fig. 9, *E* and *F*).

Discussion

These data demonstrate that while myristylation of a viral oncogene is independent of its ability to transform and immortalize cells in tissue culture, its role in vivo is crucial for tumorigenesis. Myristylated FBR–induced tumors are osteosarcomas with features of chondrosarcoma, rhabdomyosarcoma, and fibrosarcoma. The nonmyristylated mutant G2A-R induced tumors are liposarcomas. The presence of the myristoyl moiety on FBR protein allows malignant mesenchymal cells to enter and disrupt multiple differentiation pathways leading to tumors with features of osteosarcomas, chondrosarcomas, rhabdomyosarcomas, and liposarcomas. But nonmyristylated FBR disrupts the differentiation of a single cell lineage leading to liposarcomas. The differentiation pattern of osteocytes, chondrocytes, and myocytes are not disrupted and therefore appear normal in the G2A-R transgenic mice. Although we do not detect the level of lipid-accumulating adipocytes in the FBR osteosarcomas as in the G2A-R liposarcomas, there are a high number of fibroblasts and primitive mes-
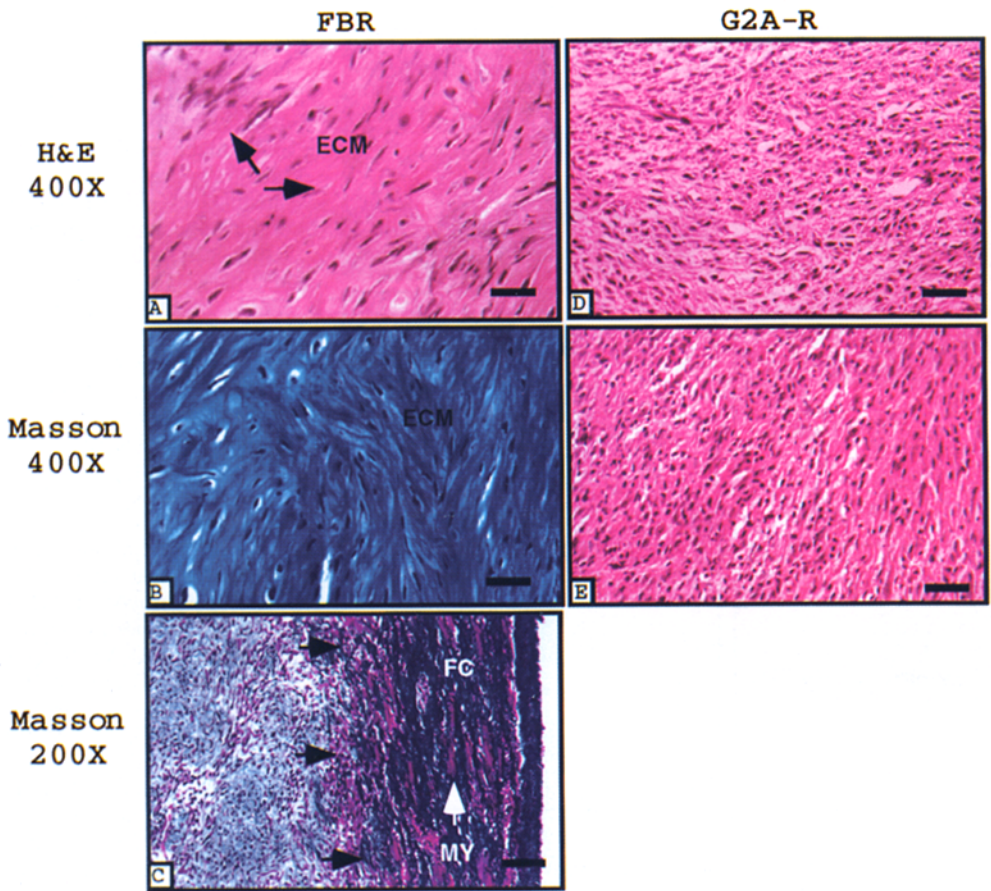
Figure 8. Collagen-rich extracellular matrix present in FBR tumors, but not G2A-R tumors. (*A*) Extracellular matrix component of FBR tumors. H&E stain of FBR tumor section reveals ECM within the soft tissue component of FBR tumors. Arrows mark whorling pattern characteristic of collagen fibrils typically found in ECM. 400 magnification. (*B*) Masson trichrome stain of FBR tumor. FBR tumors were fixed, sectioned, and stained as described in Materials and Methods. Masson trichrome stains nuclei black, cytoplasm red, and collagen fibrils blue. Note the abundance of collagen staining throughout the extracellular matrix (ECM). 400 magnification. (*C*) Masson trichrome stain at FBR tumor periphery. This section reveals the increased collagen staining observed within the fibrous capsule (*FC*) at the periphery of FBR tumors. Dark arrows demarcate the border of collagen expression in the FBR tumor capsule. White arrow notes the presence of myo-

cytes (*MY*) within the tumor capsule. 400 magnification. (*D*) G2A-R tumor devoid of ECM. H&E stain demonstrates the absence of ECM throughout the highly cellular G2A-R liposarcoma. Compare this with the ECM seen in FBR tumors in Fig. 8 *A*. 400 magnification. (*E*) Masson trichrome stain of G2A-R tumor. G2A-R tumors were fixed, sectioned, and stained as described in Materials and Methods. Note the absence of collagen staining within the G2A-R liposarcomas. Red staining is reflective of the abundance of cytoplasm within the highly cellular G2A-R tumors. 400 magnification. Bars: (*A, B, D,* and *E*) 10 μm; (*C*) 20 μm.

enchymal cells (Fig. 6 *G*), which have also been seen in FBR retrovirus-induced tumors (Price et al., 1972; Finkel et al., 1975; Ward and Young, 1976). These primitive mesenchymal cells may represent preadipocytes which are blocked from entering the adipocyte differentiation pathway (Fig. 10). FBR v-fos transformed tumor cells also exist in an extracellular matrix rich in collagen III that is transcriptionally activated by FBR v-fos (Setoyama et al., 1986*a, b*; Jotte et al., 1994). Such an environment may alter programmed cellular differentiation and allow FBR transformed cells to disrupt multiple differentiation pathways (Liau et al., 1985; Yoakum et al., 1985; Coppola and Cole, 1986).

The indistinguishable efficacy by which FBR and G2A-R cause immortalization indicates that myristylation is not necessary for cellular transformation to occur. Other regions within the FBR protein must be responsible for this initial step toward tumorigenicity. Fos sequences within FBR are a likely candidate for its immortalizing features, as unregulated expression of Fos has been shown to overcome the limited proliferative capacity of different cell lineages causing transformation (Jenuwein and Müller, 1987; Lassar et al., 1989). Although Fos sequences may initiate tumorigenesis by causing cellular transformation, these se-

quences are not the sole determinant of the differentiation pathways followed by the transformed cells. This is evidenced by the different predominant lineages observed in the FBR and G2A-R tumors. Myristylation of FBR protein defines which differentiation pathways will be disrupted. Thus, it would appear that the parameters which dictate cellular growth and immortalization are dependent upon Fos sequences, and the differentiation patterns of FBR transformed cells are dependent upon myristylation.

The mechanisms by which FBR and nonmyristylated G2A-R transformed cells disrupt differentiation remains unknown. Perhaps myristylation of FBR endows it with a novel transcriptional activity or function which disrupts the differentiation pathway of various cell lineages. Previous work in our lab and other's has examined FBR's myristylation-dependent transcriptional activity of the collagen III gene (Setoyama et al., 1986*a, b*; Jotte et al., 1994). Collagen III expression is markedly down-regulated during the differentiation of adipocytes (Weiner et al., 1989; Jotte et al., 1994). Collagen III's expression is shut off by day two of 3T3-L1 adipocyte differentiation (Jotte et al., 1994). 3T3-L1 cells stably transfected with FBR demonstrate a disruption of this expression pattern, whereas G2A-R stably transfected 3T3-L1 cells demonstrate a normal col-
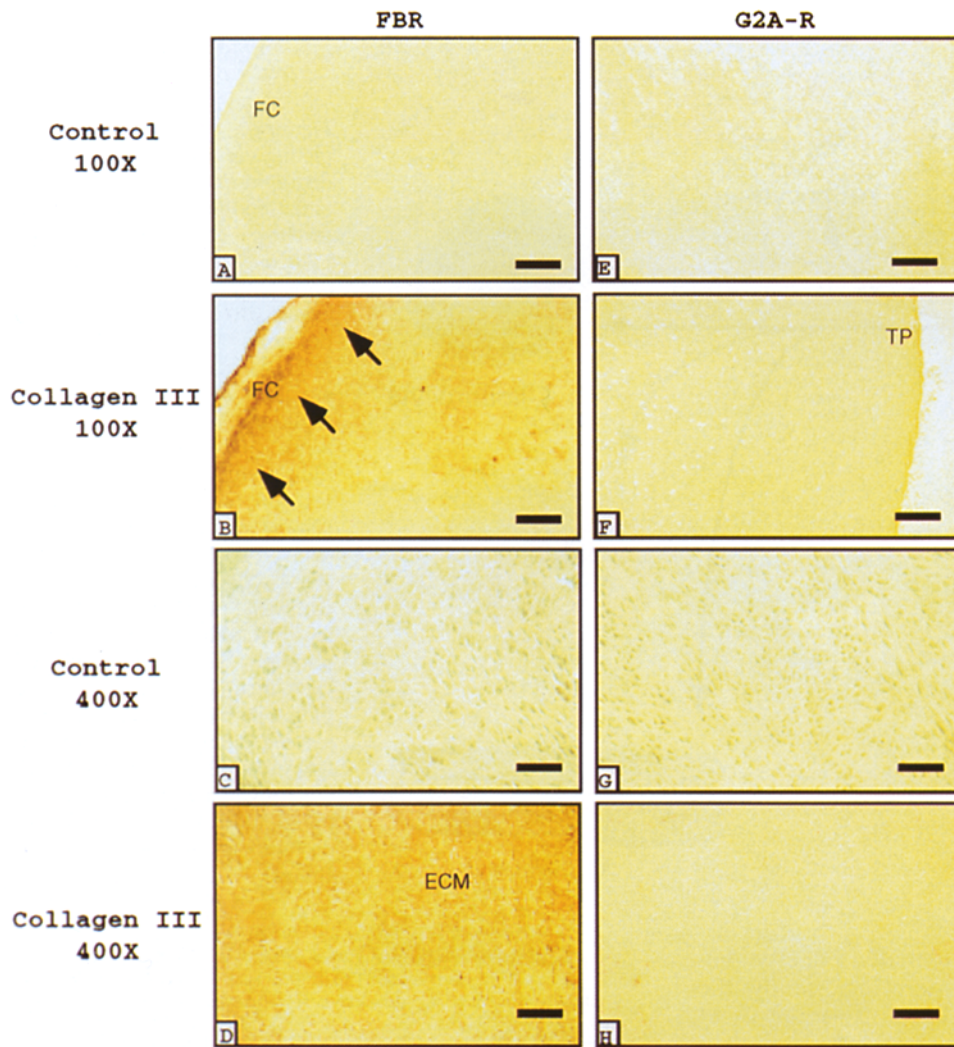
Figure 9. Collagen III expression in FBR and G2A-R tumors. (*A*) FBR control collagen III stain at tumor periphery. FBR tumors were fixed, sectioned, and stained as described in Materials and Methods. Collagen III positive staining is represented by an immunoperoxidase generated brown color. Section represents the background staining pattern for the collagen III antibody observed in FBR tumor sections at the fibrous capsule (*FC*). (*B*) Collagen III staining seen in the periphery of FBR tumors. Arrows demarcate the border of collagen III expression within the fibrous capsule (*FC*). Also note the overall increase in generalized staining for collagen III throughout the tumor section. (*C*) FBR control collagen III stain at higher magnification. Section represents the background immunoperoxidase staining pattern for the collagen III antibody observed within the FBR tumor. (*D*) FBR collagen III staining pattern at higher magnification. Note the marked staining for collagen III within the ECM of the FBR tumor. (*E*) G2A-R control collagen III stain at the tumor periphery. Section represents the background immunoperoxidase staining pattern for the collagen III antibody observed near the periphery of the G2A-R tumor. (*F*) Collagen III staining seen in the periphery of G2A-R tumors. Note the lack of enhanced collagen III staining at the periphery of G2A-R tumors compared to FBR tumors in *B*. Also note the overall decreased expression of collagen III throughout the G2A-R tumor. (*G*) G2A-R control collagen III stain at higher magnification. Section represents the background immunoperoxidase staining pattern for the collagen III antibody observed within the G2A-R tumor. (*H*) G2A-R collagen III staining pattern at higher magnification. Note the lack of staining for collagen III in the G2A-R liposarcoma. Compare this section with that of the FBR tumor in Fig. 9 *D*. Bars: (*A*, *B*, *E*, and *F*) 40 μm; (*C*, *D*, *G*, and *H*) 10 μm.

lagen III expression pattern (Abbott, D., and J.T. Holt, unpublished data). Novel FBR transcriptional properties such as this may activate genes crucial to the disruption of specific cell lineage differentiation pathways. Such a phenomenon is mimicked by fibroblasts treated with the DNA methylation inhibitor, 5-azacytidine (Chiang, 1981), which enables them to differentiate into chondrocytes, myocytes, and adipocytes (Sager and Kovac, 1982). Absence of myristylation may eliminate these novel FBR properties, restoring FBR's activity to that of its cellular homologue, c-Fos.

Earlier data has demonstrated that the known molecular mechanisms of c-Fos are restored in FBR v-fos when its myristylation site is disrupted (Kamata and Holt, 1992; Kamata et al., 1992; Jotte et al., 1994). A restoration of transcriptional properties in G2A-R (so that it behaves as the normal cellular Fos protein) may allow the transformed cells to proceed down the differentiation pathway of the adipocyte lineage and leave other differentiation pathways intact. Many studies implicate Fos protein as playing a role in modulating adipocyte differentiation-specific gene expression (Distel et al., 1987; Rauscher et al., 1988; Herrera et al., 1989; Barcellini-Couget et al., 1993). Fos sequences within FBR may allow transformed cells to proceed down the adipocyte lineage, and lack of myristylation prevents FBR from disrupting multiple differentiation pathways.

Another striking myristylation-dependent feature is the malignant nature of the FBR tumors compared to that of the G2A-R tumors. Not only do a greater number of FBR transgenic mice develop tumors, but they also die from their tumor burden. This does not occur in the G2A-R transgenic mice. Myristylation endows FBR with a greater tumorigenic and malignant potential compared to non-myristylated G2A-R. This correlates with data observed with c-Fos transgenic mice which present with benign tu-
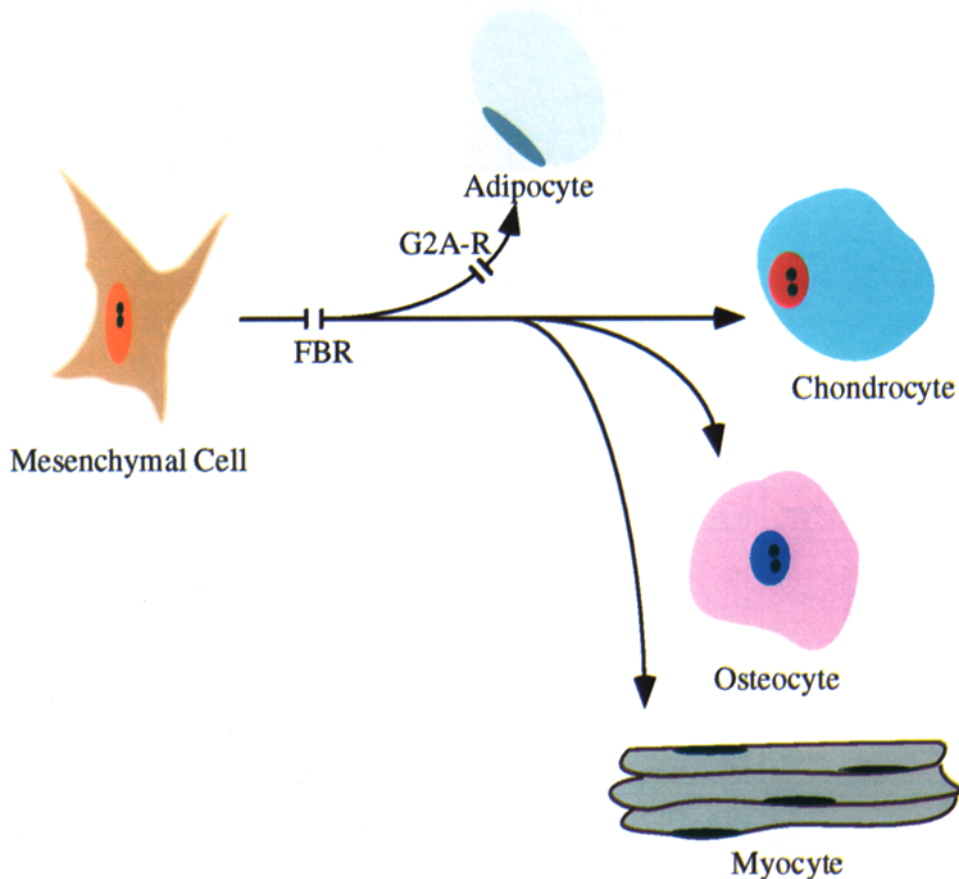
Figure 10. Schematic model depicting sites of FBR and G2A-R disruption of cell-specific differentiation lineages. Diagram represents a mechanism by which FBR may disrupt the differentiation pattern of multiple cell lineages. Broken lines represent the points at which either FBR or G2A-R disrupt normal differentiation. Myristylated FBR disrupts the differentiation pathways of four cell lineages (adipocytes, chondrocytes, osteocytes, and myocytes) early, leading to malignant tumors. When FBR is not myristylated (*G2A-R*), the differentiation pathways of chondrocytes, osteocytes, and myocytes proceed normally. Nonmyristylated G2A-R still disrupts the differentiation pathway of the adipocyte, causing liposarcomas. However, liposarcomas are a tumor of lesser malignant potential (compared to osteosarcomas, chondrosarcomas, and rhabdomyosarcomas).

mors, consisting primarily of differentiated bone-synthesizing cells (Rüther et al., 1987). More importantly, the large number of primitive mesenchymal cells and ECM observed in the FBR transgenic mouse tumors as well as in v-*fos* retrovirus-induced tumors (Price et al., 1972; Ward and Young, 1976) are absent in Fos and G2A-R transgenic mouse tumors (Wagner et al., 1987). Surroundings rich in ECM may provide the proper environment essential for the malignant nature of the FBR-induced tumors.

This data indicates a significant in vivo role of FBR myristylation that dictates the disrupted differentiation patterns of transformed mesenchymal cells. While the exact molecular mechanisms of this alteration in differentiation remains unknown, the in vivo transgenic data directly correlates with the observations of FBR molecular mechanisms in vitro. Future studies need to examine FBR's molecular properties that determine differentiation to further define how transformed cells progress to tumor formation.

References

Barcellini-Couget, S., A. Pradines-Figueres, P. Roux, C. Dani, and G. Ailhaus. 1993. The regulation by growth hormone of lipoprotein lipase gene expression is mediated by c-fos protooncogene. *Endocrinology.* 132:53–60.

Chiang, P.K. 1981. Conversion of 3T3-L1 fibroblasts to fat cells by an inhibitor of methylation: effect of 3-deazaadenosine. *Science (Wash. DC).* 211:1164–1166.

Chirgwin, J.M., A.E. Przbyla, R.J. MacDonald, and W.J. Rutter. 1979. Isolation of biologically active ribonucleic acid from sources enriched in ribonuclease. *Biochemistry.* 18:5294.

Coppola, J.A., and M.D. Cole. 1986. Constituitive c-myc oncogene expression blocks mouse erythroleukemia cell differentiation but not commitment. *Nature (Lond.).* 320:760–763.

Curran, T., and I.M. Verma. 1984. FBR v-fos murine oseteosarcoma virus. I. Molecular analysis and characterization of a 75,000-Da gag-fos fusion product. *Virology.* 135:218–228.

Distel, R.J., H.-S. Ro, B.S. Rosen, D.L. Groves, and B.M. Spiegelman. 1987. Nucleoprotein complexes that regulate gene expression in adipocyte differentiation: direct participation of c-fos. *Cell.* 49:835–844.

Finkel, M.P., C.A. Reilly, Jr., and B.O. Biskis. 1975. Viral etiology of bone cancer. *Front. Radiat. Ther. Oncol.* 10:28–39.

Graham, F., and A. van der Eb. 1973. A new technique for the assay of infectivity of human adenovirus 5 DNA. *Virology.* 52:456–467.

Herrera, R., H.S. Ro, G.S. Robinson, K.G. Xanthopoulos, and B.M. Spiegelman. 1989. A direct role for C/EBP and the AP-1-binding site in gene expression linked to adipocyte differentiation. *Mol. Cell. Biol.* 9:5331–5339.

Hogan, B., F. Constantini, and E. Lacy. 1986. Manipulating the Mouse Embryo: a Laboratory Manual. Cold Spring Harbor Press, Plainview, NY.

Jenuwein, T., and R. Müller. 1987. Structure-function analysis of fos protein: a single amino acid change activates the immortalizing potential of v-fos. *Cell.* 48:647–657.

Jenuwein, T., D. Miller, T. Curran, and R. Müller. 1985. Extended life span and tumorigenicity of nonestablished mouse connective tissue cells transformed by the fos oncogene of FBR-MuSV. *Cell.* 41:629–637.

Jotte, R.M., N. Kamata, and J.T. Holt. 1994. Myristylation dependent transactivation by FBR v-fos is regulated by C/EBP. *J. Biol. Chem.* 269:16383–16396.

Kamata, N., and J.T. Holt. 1992. Inhibitory effect of myristylation on transrepression by FBR (Gag-Fos) protein. *Mol. Cell. Biol.* 12:876–882.

Kamata, N., R.M. Jotte, and J.T. Holt. 1991. Myristylation alters DNA-binding activity and transactivation of FBR (gag-fos) protein. *Mol. Cell. Biol.* 11: 765–772.

Lassar, A.B., M.J. Thayer, R.W. Overell, and H. Weintraub. 1989. Transformation by activated ras or fos prevents myogenesis by inhibiting expression of MyoD1. *Cell.* 58:659–667.

Lee, C.K., E.W. Chan, C.A. Reilly, V.A. Pahnke, G. Rockus, and M.P. Finkel. 1979. In vitro properties of FBR murine osteosarcoma virus. *Proc. Soc. Exp. Biol. Med.* 162:214–220.

Liau, G., Y. Yamada, and B. de Crombrugghe. 1985. Coordinate regulation of the levels of type III and type I collagen mRNA in most but not all mouse fibroblasts. *J. Biol. Chem.* 260:531–536.

Meijlink, F., T. Curran, A.D. Miller, and I.M. Verma. 1985. Removal of a 67 base pair sequence in the non-coding region of proto-oncogene fos converts it to a transforming gene. *Proc. Natl. Acad. Sci. USA.* 82:4987–4991.

Michiels, L., J.R. Maisin, F.S. Pedersen, and J. Merregaert. 1984. Characterization of the FBR-murine osteosarcoma virus complex: FBR-MuSV encodes a fos-derived oncogene. *Int. J. Cancer.* 33:511–517.

Price, C.H.G., M. Moore, and D.B. Jones. 1972. FBJ virus-induced tumours in mice. A histopathological study of FBJ virus tumours and their relevance to murine and human osteosarcoma. *Br. J. Cancer.* 26:15–27.

Rauscher, F.J., III, L.C. Sambucetti, T. Curran, R.J. Distel, and B.M. Spiegelman. 1988. Common DNA binding sites for fos protein complexes and transcription factor AP-1. *Cell.* 42:471–480.

Rüther, U., C. Garber, D. Komitowski, R. Müller, and E.F. Wagner. 1987. Deregulated c-*fos* expression interferes with normal bone development in transgenic mice. *Nature (Lond.).* 325:412–416.

Sager, R., and P. Kovac. 1982. Preadipocyte determination either by insulin or by 5-azacytidine. *Proc. Natl. Acad. Sci. USA.* 79:480–484.

Setoyama, C., R. Frunzio, G. Liau, M. Mudryj, and B. de Crombrugghe. 1986a. Transcriptional activation encoded by the v-fos gene. *Proc. Natl. Acad. Sci. USA.* 83:3213–3217.

Setoyama, C., A. Hatamochi, B. Peterkofsky, W. Prather, and B. de Crombrugghe.

1986b. v-fos stimulates expression of the alpha 1 (III) collagen gene in NIH 3T3 cells. *Bio. Biophys. Res. Commun.* 136:1042–1048.

Silbermann, M., J. Schmidy, E. Livne, K. von der Mark, and V. Erfle. 1987. In vitro induction of osteosarcoma-like lesions by transformation of differentiating skeletal precursor cells with FBR osteosarcoma virus. *Calcif. Tissue Int.* 44:208–217.

Thompson, M.E., R.A. Jensen, P.S. Obermiller, D.L. Page, and J.T. Holt. 1995. Decreased expression of BRCA1 accelerates growth and is often present during sporadic breast cancer progression. *Nat. Genet.* 9:444–450.

Van Beveren, C., S. Enami, T. Curran, and I.M. Verma. 1984. FBR v-fos murine osteosarcoma virus. II. Nucleotide sequence of the provirus reveals that the genome contains sequences acquired from two cellular genes. *Virology.* 135:229–243.

Ward, J.M., and D.M. Young. 1976. Histogenesis and morphology of periosteal sarcomas induced by FBJ virus in NIH-Swiss mice. *Cancer Res.* 36:3985–3992.

Weiner, F.R., A. Shah, P.J. Smith, and C.S. Rubin. 1989. Regulation of collagen gene expression in 3T3-L1 cells. Effects of adipocyte differentiation and tumor necrosis factor alpha. *Biochemistry.* 28:4094–4099.

Wilson, T., and R. Treisman. 1988. fos C-terminal mutations block downregulation of c-fos transcription following serum stimulation. *EMBO (Eur. Mol. Biol. Organ.) J.* 7:4193–4202.

Yoakum, G.H., J.F. Lechner, E.W. Gabrielson, B.E. Korba, L. Malan-Shibley, J.C. Willey, A.M. Shamsuddin, B.F. Trump, and C.C. Harris. 1985. Transformation of human bronchial epithelial cells transfected by Harvey ras oncogene. *Science (Wash. DC).* 227:1174–1179.